ICW Note 1914
December 1988

nota

instituut voor cultuurtechniek en waterhuishouding, wageningen

NEW EMPIRICAL ASPECTS OF THE BOWEN-RATIO ENERGY BALANCE METHOD

A study of evaporation losses in arid regions

ing. W.G.M. Bastiaanssen

Nota's (Notes) of the Institute are a means of internal communication and not a publication. As such their contents vary strongly, from a simple presentation of data to a discussion of preliminary research results with tentative conclusions. Some notes are confidential and not available to third parties if indicated as such

NOTA/1914

CONTENTS

NOTA/1914

CONTENTS

1. INTRODUCTION

Remote sensing techniques offer the possibility to estimate evapotranspiration for relatively large areas if ground measurements are available. This technique is applied in an investigation towards the natural evaporation losses of fossil groundwater in vast depressions of the Saharian belt. In the framework of this mapping evaporation project, in situ measurements of energy balance terms were made.

The evapotranspiration can be evaluated by means of the Bowen-ratio method. This rather simple technique is very useful to determine the actual rate of evapotranspiration with field observations. Fieldwork was carried out near Bir Qifar (lat. 29°·33'long. 26°·58') in the Qattara depression, Western desert of Egypt, during May through July 1988. Although the analysis of evapotranspiration and other energy terms will be focussed on this data set, former field observations in the Qattara depression (1987), will be applied.

In this report, an analysis of the measured energy fluxes and empirical relationships among them is presented.

Furthermore, empirical regression constants of well known formulae like Brunt, Brutsaert, Swinbank and de Bruin are derived.

A procedure is outlined to map net radiation with satellite observations. Estimates of bare soil evaporation will be obtained on the basis of observed relationships between net radiation and soil heat flux. Values of actual evaporation in deserts are finally given.

2. BOWEN-RATIO ENERGY BALANCE METHOD

Energy fluxes entering and leaving the ideal surface at the boundary between earth and atmosphere must balance with each other. Energy fluxes entering the surface are counted positive. The surface energy balance reads:

$$R_n + G_0 + H + LE = 0 \qquad [2.1]$$

Where LE ($W.m^{-2}$) is the latent heat flux, G_0 ($W.m^{-2}$) the soil heat flux at the surface, H ($W.m^{-2}$) the sensible heat flux and R_n ($W.m^{-2}$) the amount of net radiation.
The sensible and latent heat flux can be related to the vertical gradient of respectively temperature and vapour concentration and can be expressed as:

$$LE = - \frac{\rho_a . C_p}{\gamma . R_{av}} [e(0) - e(z)] \qquad [2.2]$$

$$H = - \frac{\rho_a . C_p}{R_{ah}} [T(0) - T(z)] \qquad [2.3]$$

with:

ρ_a	= air density	($kg.m^{-3}$)
C_p	= air specific heat at constant pressure	($J.kg.K^{-1}$)
R_{av}	= resistance to transport of vapour through air	($s.m^{-1}$)
R_{ah}	= resistance to transport of heat through air	($s.m^{-1}$)
e	= actual vapour pressure	(mbar)
T	= actual temperature	(K)
γ	= psychrometric constant	($mbar.K^{-1}$)

Assuming that $R_{av} = R_{ah}$, which in most cases holds true, the ratio H/LE can be written as:

$$\beta = \gamma \frac{[T(0)-T(z)]}{[e(0)-e(z)]} \qquad [2.4]$$

Where β is named Bowen ratio, after BOWEN (1924) who first proposed this concept. Combination of eq. [2.1] and [2.4] yields:

$$LE = - \frac{R_n - G_0}{1 - \beta} \qquad [2.5]$$

The energy balance equation form [2.1] is that it implies that water evaporates at the surface. This only holds true for soils with a relatively wet surface. However, when a barren surface dries out, like in arid regions, phase transition of water will occur inside the soil. MENENTI (1984) defined an evaporation front at some depth in the soil as based on the interrelation between vapour flow regime and pore size. Without going into details, it was shown that at a certain water content, the exit velocity of vapour molecules out of small pores increases and causes an increment in the soil water diffusivity at lower water content.
With internal evaporation, the soil heat flux at the surface (G_0) supplies the energy required for it. The energy balance at the evaporation front can be written as:

$$G_0 - W_e - LE - G_e = 0 \qquad [2.6]$$

with:

$$W_e = \int_0^{Z_e} C \frac{\partial T}{\partial t} dz = \text{heat storage } (W.m^{-2}) \qquad [2.7]$$

LE = latent heat flux ($W.m^{-2}$)

G_e = soil heat flux at the evaporation front ($W.m^{-2}$)

When the evaporation is potential (evaporation front at surface level), G_0 accounts for soil heat exchange only. If the actual evaporation becomes less than potential evaporation (evaporation front inside the soil), LE is a part of G_0.
With internal evaporation, the latent heat flux through the soil is identical to the latent heat flux in the air, eq. [2.5] can be rewritten as:

$$LE = - \frac{R_n - G_e + W_e}{1 - \beta} \qquad [2.8]$$

3. NET RADIATION

3.1. REVIEW

The net radiation flux absorbed by the surface is the most important term of the surface energy balance. Although only measured values of net radiation are adequately accurate, it is useful to derive net radiation with empirical relationships when net radiometers are not available. That makes it possible to evaluate the net radiation by means of other observations, such as calibrated pyranometers, temperature and humidity sensors and/or spectral radiance data collected by satellites. The spacial distribution of net radiation can be assessed for different surface types when remote sensing techniques are applied.
Net radiation equals the sum of net shortwave (0.3-2.8 μm), R_{sn} and net longwave radiation R_{ln} (8-14 μm):

$$R_n = R_s\downarrow - R_s\uparrow + R_l\downarrow + R_l\uparrow \qquad [3.1]$$

The arrow indicate respectively downwelling and upwellinge radiation. The net shortwave radiation, which appears to be the major component of net radiation, depends mainly on the surface reflectance, while the incoming shortwave (solar) radiation is rather uniform for large arid areas. The incoming shortwave radiation decreases with the progress of fractional cloudiness. The incoming shortwave radiation can be estimated by means of a simple equation:

$$R_s\downarrow = (a+b\ n/N)\ R_a \qquad [3.2]$$

where R_a is the extra terrestrial radiation, n/N the fractional sunshine duration and a and b are empirical constants, mostly near 0.25 and 0.50 respectively (DOORENBOS and PRUITT, 1977).
The net shortwave radiation can be written as:

$$R_{sn} = (1-\alpha_o)\ R_s\downarrow \qquad [3.3]$$

where α_o(-) is the surface reflectance.

More troublesome is the determination of the net longwave radiation. The Stefan-Boltzmann equation can be applied to obtain both the downwelling $R_{l\downarrow}$ and upwelling $R_{l\uparrow}$ longwave radiation. This requires the definition of an apparent emissivity of the atmosphere, ϵ':

$$R_{ln} = - \epsilon\sigma T_0^4 + \epsilon'\sigma T_a^4 \qquad [3.4]$$

With T_o and T_a being respectively the surface and air temperature (K). The soil surface may not be considered as a black body radiator. The spectral surface emissivity of bare soils is therefore governed by the absorption coefficients and their dependence on wavelength. Furthermore, longwave surface emissivity increases linear with soil water content (TEN BERGHE, 1986). Considering the band width of the thermal infrared channel of the Thematic Mapper (band 6; 10.5-12.5 μm), the range of surface emissivity for deserts becomes ϵ = 0.96-0.98. TAKASHIMA and MASUDA (1987) showed that emissivity of quartz and dust powders increases monotonically with the particle size in the region 10-17 μm.
A quartz powder having particle size in the range 20 to 7400 μm has an emissivity of ϵ = 0.971. The typical emissivity for vegetation is somewhat lower ϵ = 0.90-0.98 (LILLESAND and KIEFER, 1987). The reflection of longwave incoming radiation can be ignored, because only wavelengths between 2.8 and 3.0 μm will contribute to reflection.
The apparent emissivity concept implies that the atmosphere is considered as a grey body at the screen height temperature. Apparent emissivity of clear skies can conveniently be related with either actual vapour pressure (BRUNT, 1932), air temperature (SWINBANK, 1963) or a combination of them (BRUTSAERT, 1975).
A successful formula to account for apparent emissivity used in practice, was given by Brunt, who assumed the form of his formula analogue with unsteady heat conduction and thermal diffusivity, namely absorption as a function of the square root of vapour pressure (mbar):

$$\epsilon' = a + b\sqrt{e_{act}} \qquad [3.5]$$

The required constants for eq. [3.5] are derived for different places on earth (see Table 3.1):

Table 3.1. Constants, a, b in Brunt's formula for longwave clear sky radiation

a	b	Source	Location
0.52	0.065	Brunt (1932)	England
0.68	0.036	Anderson (1954)	Oklahoma
0.66	0.039	Goss and Brooks (1956)	California
0.645	0.048	De Coster and Schuepp (1957)	Kinshasa
0.61	0.050	Budyko (1958)	-
0.605-0.75	0.048	Sellers (1965)	-
0.60 -0.75	0.017-0.057	Wartena et al. (1973)	-
0.51 -0.60	0.059-0.065	Unsworth and Monteith (1975)	-
0.66	0.044	Doorenbos and Pruitt (1977)	Tropics
0.62	0.035	Stroosnijder and van Heemst (1982)	-

note: after BRUTSAERT (1975) and TEN BERGHE (1986)

Brutsaert showed that the apparent emissivity under a clear sky can be empirically related with the actual vapour pressure (mbar) and air temperature (K):

$$\epsilon' = 1.24\left(\frac{e_{act}}{T_a}\right)^{1/7} \qquad [3.6]$$

Although the equation depends on both vapour pressure, and temperature, the value of ϵ' is more sensitive to variations in e_a than in T_a.
Independent work done by Swinbank gave another empirical relationship:

$$\epsilon' = 0.398\ 10^{-5}\ T_a^{\ 2.148} \qquad [3.7]$$

In the presence of clouds, the apparent clear sky emissivity has to be corrected with the [1-d(1-n/N)] term, where d = fractional cloud cover and n/N = relative sunshine duration.

3.2.DETERMINATION OF NEW COEFFICIENTS OF APPARENT EMISSIVITY FORMULAE

The apparent emissivity can be calculated with different formulae as shown in the preceding section. To obtain ϵ'-values, the empirical coefficients of these formulae must be obtained under local conditions. It was possible to determine the downwelling longwave radiation term according eq. [3.1], since net radiation was measured by a net radiometer, the net shortwave radiation was observed by means of a set dynamometers and the upwelling

longwave radiation was measured by a thermal infrared radiometer. Finally, ϵ' can be obtained by inversion of Stefan Boltzmann's law:

$$\epsilon' = \frac{R_n - R_s^{\downarrow} + R_s^{\uparrow} + R_l^{\uparrow}}{\sigma . T_a^4} \qquad [3.8]$$

Mean daily values of the indirectly measured effective apparent emissivity, spread over three field campaigns are listed in Table 3.2.
The mean value for day and nighttime becomes $\overline{\epsilon}'$day = 0.848 and $\overline{\epsilon}'$night = 0.804 respectively. Yet, the ratio of $\overline{\epsilon}'$night/$\overline{\epsilon}'$day is approximately equal to 0.95. It can be seen that during the day the observed range is $\overline{\epsilon}'$day = 0.689-0.987 while at night smaller range could be noticed; $\overline{\epsilon}'$night =

Table 3.2. Observed daytime and nighttime apparent emissivity at 2.0 m height; fieldwork 1987-1988

Day			Night		
Date	Day	number of datapoints	Date	Night	number of datapoints
11/3/87	0.848	9	11/3/87	0.732	15
12/3/87	0.987	12	12/3/87	0.721	10
13/3/87	0.881	23	14/3/87	0.799	6
15/3/87	0.892	66	15/3/87	0.797	7
16/3/87	0.904	8	11/11/87	0.721	7
4/11/87	0.689	15	11/6/88	0.867	18
5/11/87	0.815	60	12/6/88	0.803	34
6/11/87	0.846	89	13/6/88	0.801	8
11/11/87	0.760	83	14/6/88	0.773	39
12/11/87	0.790	99	15/6/88	0.800	51
13/11/87	0.808	26	16/6/88	0.731	5
11/6/88	0.887	97	18/6/88	0.838	60
12/6/88	0.821	133	19/6/88	0.864	78
13/6/88	0.858	23	20/6/88	0.822	52
14/6/88	0.884	101	21/6/88	0.799	76
15/6/88	0.839	144	22/6/88	0.746	29
16/6/88	0.791	35	23/6/88	0.784	53
17/6/88	0.886	88	24/6/87	0.796	95
18/6/88	0.871	113	25/6/88	0.806	40
19/6/88	0.901	31			
20/6/88	0.850	125			
21/6/88	0.861	124			
22/6/88	0.756	37			
23/6/88	0.873	118			
24/6/88	0.871	134			
25/6/88	0.857	101			

less than unity, thus supporting the use of field measurements as done. These measurements of ϵ' have been applied to obtain new values of the coefficients in the formulae mentioned in Paragraph 3.1. This provides a description consistent with desert observations at any timestep. Since air humidity was measured with very accurate instruments in 1988 only, the required constants were determined at any time period for that field campaign only. The resultant formulae arranged with revised constants for day and night are:

	Day	night
Brunt	$\epsilon' = 0.72 + 0.046 \sqrt{e_{act}}$	$\epsilon' = 0.61 + 0.068 \sqrt{e_{act}}$
Brutsaert	$\epsilon' = 1.111 \ (e_{act}/T_a)^{0.0728}$	$\epsilon' = 1.214 \ (e_{act}/T_a)^{0.115}$
Swinbank	$\epsilon' = 0.248 \ 10^{-5}.T_a^{2.237}$	$\epsilon' = 0.149 \ 10^{+4}.T_a^{-1.318}$

Table 3.3 presents the root mean square errors (RMS) of computed apparent emissivity against measured values of ϵ'.

Table 3.3. Root mean square values of observed and calculated apparent emissivity at any timestep; fieldwork 1988

Date	Day			Night		
	RMS (Brunt)	RMS (Brutsaert)	RMS (Swinbank)	RMS (Brunt)	RMS (Brutsaert)	RMS (Swinbank)
11/6	0.0413	0.0414	0.0508	0.0422	0.0441	0.0577
12/6	0.0382	0.0386	0.1064	0.0344	0.0373	0.0221
13/6	0.0562	0.0542	0.0236	-	-	-
14/6	0.0385	0.0571	0.1320	0.0328	0.0419	0.0171
15/6	0.0279	0.0312	0.0889	0.0068	0.0074	0.0074
16/6	0.0516	0.0540	0.0695	-	-	-
17/6	0.0598	0.0620	0.0465	-	-	-
18/6	0.0544	0.0574	0.0879	0.0770	0.0825	0.0667
19/6	0.0594	0.0573	0.0183	0.0672	0.0685	0.0651
20/6	0.0567	0.0703	0.1221	0.0281	0.0308	0.0415
21/6	0.0186	0.0182	0.0799	-	-	-
22/6	0.0969	0.0947	0.0940	0.0562	0.0444	0.0149
23/6	0.0402	0.0388	0.0580	0.0402	0.0388	0.0580
24/6	0.0628	0.0607	0.0424	0.0462	0.0427	0.0244
25/6	0.0286	0.0280	0.0541	0.0640	0.0574	0.0254
aver.	0.0487	0.0509	0.0716	0.0450	0.0450	0.0364

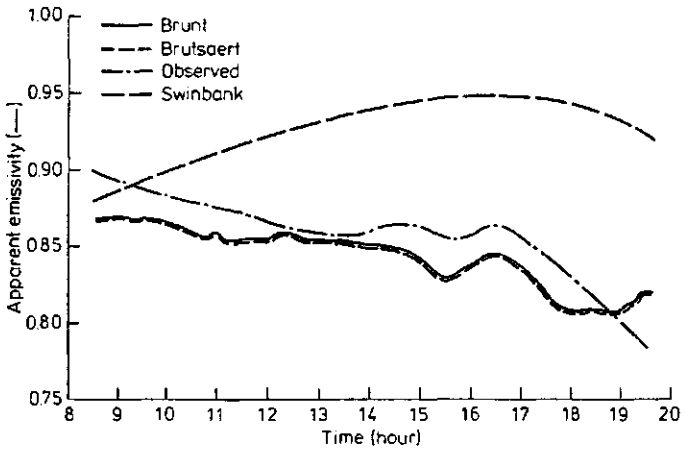

Fig. 3.1. Observed and calculated values for apparent emissivity according various emissivity models; Bir Qifar-4, 21 June 1988

The Brunt-type formula (RMS = 0.0487) gave the lowest root mean square error while the Swinbank-type formula gave the largest error (RMS = 0.0716) (Fig.3.1).
It can be concluded that the best approach is by applying the Brunt-type formula, having coefficients obtained independently with night- and daytime measurements.

3.3. ATMOSPHERIC CONDITIONS

Interaction of electromagnetic radiation with the atmosphere occurs through absorption and scattering. The scattering processes can be split up into Rayleigh and Mie scattering.
Rayleigh scattering occurs with visible light when the effective diameter of air molecules is many times smaller than the wavelength. Mie scattering on the other hand, occurs with particles having the same diameter as the radiation wavelength, such as dust, aerosols and water vapour. So, with increasing vapour and dust concentration, scattering increases and affect the direction and intensity of energy propagation. This results in a decrease of direct energy reaching the surface.
The effect of atmospheric conditions on the surface energy balance is two-fold. Atmospheric water vapour and aerosols affect both surface reflectance and apparent emissivity. These scattering and absorption interactions can

be indicated by the ratio of diffuse to total radiation, the optical depth of the atmosphere and the fractional cloudiness. These indicators can be easily measured in local conditions. The results of these measurement are work out in the next sections.

3.3.1. Diffuse radiation

The attenuation of atmospheric radiation at the earth surface is due to scattering, dependent on the presence of atmospheric water vapour and dust. The total radiation at the bottom of the atmosphere equals the sum of direct and diffuse radiation. The spectral ratio of diffuse radiation to total radiation ($R_{df}(\lambda)/R(\lambda)$) is the most direct measure of scattering processes. The ratio R_{swdf}/R_{sw} can be obtained by integration of the spectral ratio with respect to the wavelength in the shortwave range. The ratio R_{swdf}/R_{sw} was measured simultaneously with the apparent emissivity during the third and fourth field campaign and is presented as a weigthed mean daily value, defined according eq. [3.9], in Table 3.4. Although R_{swdf}/R_{sw} and $R_{df}(\lambda)/R(\lambda)$ are both effected by vapour and dust concentration, it is hereby emphasized that R_{swdf}/R_{sw} will not reveal the spectral dependence of the effects of water vapour and dust, as $R_{ds}(\lambda)/R(\lambda)$ does.

$$\frac{\overline{R}_{swdf}}{\overline{R}_{sw}} = \frac{\sum_{i=1}^{n} \left(\frac{R_{swdf}}{R_{sw}}\right)_i \; R_{sw,i}}{\sum_{i=1}^{n} R_{sw,i}} \qquad [3.9]$$

As can be seen, the daily ratio of $\overline{R}_{swdf}/\overline{R}_{sw}$ increases with apparent emissivity, but the low correlation coefficient ($r = 0.52$) is not very overwhelming (Fig. 3.2). So, the linear regression constants $a = 0.804$ and $b = 0.167$ are not very meaningful. In fact the low correlation is logical, because scattering of solar radiation and absorbtion/emission in the thermal infrared spectral range are very different physical processes, although both scattering and absorption increase with increasing vapour concentration. It is quite well possible that days with relative high $\overline{R}_{swdf}/\overline{R}_{sw}$ values, contain more atmospheric dust (18-22 June 1988) or clouds at high

Table 3.4. Mean observed values of apparent emissivity $\overline{\epsilon}$'day, weighted ratio of diffuse to total solar radiation $\overline{R}swdf/\overline{R}sw$ and relative sunshine duration n/N

Date	observation period	$\overline{\epsilon}$'day	$\overline{R}_{swdf}/\overline{R}_{sw}$	n/N	atmospheric condition
5/11/87	8.05-17.20	0.815	0.283	0.52	cloudy
6/11/87	7.25-16.50	0.846	0.483	0.10	cloudy
11/11/87	10.35-18.05	0.760	0.125	1.00	cloudless
12/11/87	7.05-17.15	0.790	0.254	0.88	cloudy
13/11/87	6.45- 9.35	0.808	0.251	1.00	hazy/slightly cloudy
11/ 6/88	9.10-19.30	0.887	0.453	0.54	cloudy
12/ 6/88	6.10-19.30	0.821	0.367	0.76	cloudy
13/ 6/88	6.05- 9.35	0.858	0.210	1.00	hazy/slightly cloudy
14/ 6/88	10.05-19.30	0.884	0.251	1.00	hazy/slightly cloudy
15/ 6/88	6.20-19.30	0.839	0.277	1.00	hazy/slightly cloudy
16/ 6/88	6.20-10.05	0.791	0.393	1.00	hazy
17/ 6/88	8.55-17.40	0.886	0.208	1.00	hazy/slightly cloudy
18/ 6/88	6.40-19.30	0.871	0.347	1.00	hazy
19/ 6/88	6.30- 9.50	0.901	0.464	1.00	hazy
20/ 6/88	8.25-19.30	0.850	0.425	1.00	hazy
21/ 6/88	8.40-19.30	0.861	0.333	1.00	hazy
22/ 6/88	6.20-10.05	0.756	0.435	1.00	hazy
23/ 6/88	8.40-19.30	0.873	0.165	1.00	cloudless
24/ 6/88	6.30-19.30	0.871	0.201	1.00	hazy/slightly cloudy
24/ 6/88	6.30-15.10	0.857	0.207	1.00	hazy/slightly cloudy

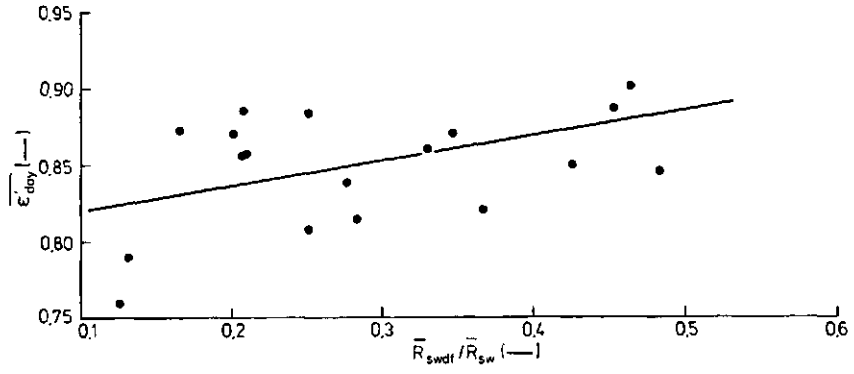

Fig. 3.2. Mean daily observed values of apparent emissivity $\overline{\epsilon}$'day versus the weigthed ratio of $\overline{R}_{swdf}/\overline{R}_{sw}$

altitudes (5-6 November 1987). The observed fractional sunshine duration (n/N) is listed to check this hypothesis. The cloud patterns (n/N) agree nicely with the field weather report (last column), which confirms again that $\overline{R}_{swdf}/\overline{R}_{sw}$ in combination with n/N is an indication for dust rather than for water vapour and not useful to relate with apparent emissivity.

3.3.2. Atmospheric transmittance

It was anticipated that the selection of R_{swdf}/R_{sw} is only convenient to account for atmospheric scattering processes e.g. due to dust. A better way of assessing the role of absorption is by making use of the transmittance of solar radiation, where the transmittance is defined as the ratio between the solar radiation at the bottom and at the top of the atmosphere respectively. The total optical depth (τ_{tot}) is calculated from atmospherical transmittance (T) according $\tau_{tot} = - \ln(T)$. Theoretically one should correlate the vapour optical depth (τ_v) with the apparent emissivity. The total optical depth $\tau_{(tot)}$ however, is the only transmittance variable observed together with the apparent sky emissivity during the fieldwork. The weighted mean values for total optical depth calculated in the form of eq. [3.9] are listed in table 3.5. All values gathered in the framework of this project are presented.

It is evident from Table 3.5 that to relate the apparent emissivity to total optical depth, a non-linear function is necessary (Fig. 3.3). Yet, the inference of $\overline{\epsilon}'$day from the total optical depth at any timestep is more trustworthy than from the ratio $\overline{R}_{swdf}/\overline{R}_{sw}$. The analytical solution in the permitted range of the total optical depth $\overline{\tau}_{tot}$ = 0.2-0.6 can be written as:

$$\overline{\epsilon}'_{day} = 1.08\ \overline{\tau}_{tot}^{0.265} \qquad [3.10]$$

which has been obtained by best-fitting the experimental data.

The spectral radiative properties of the atmosphere are the basis for atmospherical correction of satellite images. The total optical depth equals the sum of all components i.e. τ(water vapour absorption) + τ(ozon absorption) + τ(mixed gases absorption) + τ(Raleigh scattering) + τ(aerosol scatterring), where all τ are spectral quantities. These properties were both measured with an experimental type of rotating-band spectroradiometer during the fieldchecks. The instrument measures total irradiance and, when the sensor is covered by the rotating band, the dif-

Table 3.5. Mean weighted optical depth $\overline{\tau}_{tot}$ in relation with mean apparent emissivity, $\overline{\epsilon}$'day

Date	location	observed period	$\overline{\epsilon}$'day	$\overline{\tau}_{tot}$	number of datapoints
1/ 8/86	Bir Sharib	10.05-15.55	-	0.177	4
3/ 8/86	Bir Sharib	8.40-10.05	-	0.074	2
4/ 8/86	Moghra oasis	12.05-17.40	-	0.231	3
5/ 8/86	Moghra oasis	9.05-16.50	-	0.271	7
26/ 2/87	Bir Tarfawi	14.10-18.00	-	0.273	11
27/ 2/87	Bir Tarfawi	9.30-14.50	-	0.218	28
6/ 3/87	Bir Sharib	13.20-16.20	-	0.404	14
9/ 3/87	Siwa oasis	12.50-17.40	-	0.420	22
10/ 3/87	Siwa oasis	8.40-15.40	-	0.241	23
11/ 3/87	Siwa oasis	13.10-17.40	0.848	0.314	15
12/ 3/87	Siwa oasis	6.30-17.30	0.987	0.227	22
13/ 3/87	Siwa oasis	10.00-14.20	0.881	0.724	22
15/ 3/87	Siwa oasis	6.50-18.20	0.892	0.434	68
16/ 3/87	Siwa oasis	7.20-14.00	0.904	0.235	7
4/11/87	Qara oasis	15.55-17.20	0.689	0.405	11
5/11/87	Qara oasis	8.05-17.20	0.815	0.317	79
6/11/87	Qara oasis	7.25-16.50	0.846	0.377	89
8/11/87	Qattara	10.40-17.20	-	0.254	72
9/11/87	Qattara	6.35- 8.50	-	0.412	28
11/11/87	Qaneitra	10.35-17.15	0.760	0.267	80
12/11/87	Qaneitra	6.35-17.15	0.790	0.355	121
13/11/87	Qaneitra	6.45- 9.35	0.808	0.387	36
11/ 6/88	Bir Qifar-1	9.10-19.30	0.887	0.436	101
12/ 6/88	Bir Qifar-1	8.50-19.30	0.821	0.385	116
13/ 6/88	Bir Qifar-1	6.30- 9.35	0.858	0.393	26
14/ 6/88	Bir Qifar-2	10.05-19.30	0.884	0.395	107
15/ 6/88	Bir Qifar-2	6.20-19.30	0.839	0.396	158
16/ 6/88	Bir Qifar-2	6.35- 9.55	0.791	0.462	40
17/ 6/88	Bir Qifar-3	8.55-17.40	0.886	0.352	88
18/ 6/88	Bir Qifar-3	6.40-19.30	0.871	0.452	123
19/ 6/88	Bir Qifar-3	6.30- 9.50	0.901	0.574	37
20/ 6/88	Bir Qifar-4	8.25-19.30	0.850	0.438	130
21/ 6/88	Bir Qifar-4	8.40-19.30	0.861	0.408	130
22/ 6/88	Bir Qifar-4	6.30-10.00	0.756	0.531	43
23/ 6/88	Bir Qifar-5	8.40-19.30	0.873	0.366	124
24/ 6/88	Bir Qifar-5	6.30-19.30	0.871	0.363	146
25/ 6/88	Bir Qifar-5	6.30-15.25	0.857	0.330	107

fuse irradiance only. The instrumental characteristics of this so called Guzzimeter are listed in Table 3.6.

The integrated optical depth for all bands as measured with the Guzzimeter can be obtained from the spectral optical depths applying to all separate bands according:

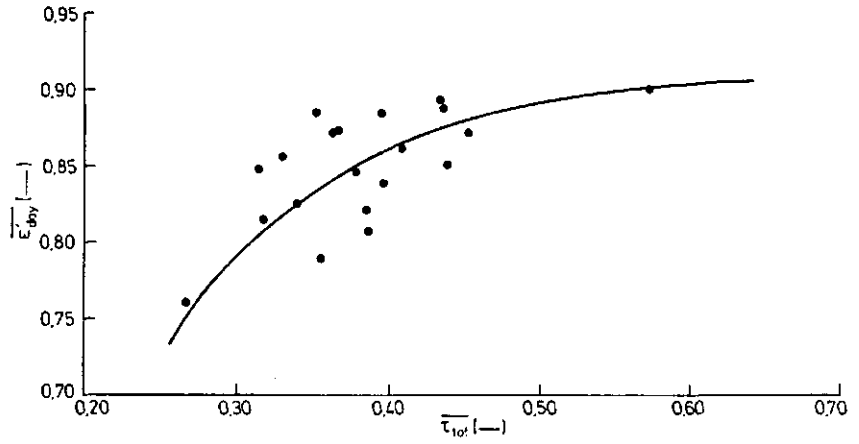

Fig. 3.3. Mean observed values of apparent emissivity, $\overline{\epsilon}$'day versus the weigted mean total optical depth, $\overline{\tau}_{tot}$

Table 3.6. Instrumental characteristics of the Guzzi rotating-band spectroradiometer

Band	Wavelength (nm)	Radiation flux at top of atmosphere ($mW.cm^{-2}$)	Weighing coefficient
1	379.5 - 414.5	4.828	0.190
2	426.5 - 441.5	2.527	0.100
3	484.0 - 504.0	3.900	0.154
4	504.0 - 524.0	3.717	0.147
5	533.5 - 558.5	4.369	0.172
6	666.5 - 681.5	2.177	0.086
7	726.5 - 741.5	1.926	0.076
8	921.0 - 931.0	0.864	0.034
9	1007.5 - 1022.5	1.062	0.042

$$\tau_{(0.3\text{-}2.8\ \mu m)} = 0.190\ \tau_1 + 0.100\ \tau_2 + 0.154\ \tau_3 + 0.147\ \tau_4 + 0.172\ \tau_5 + 0.086\ \tau_6 + 0.076\ \tau_7 + 0.034\ \tau_8 + 0.042\ \tau_9 \quad [3.11]$$

where all optical depths are obtained from the ratio of direct irradiance at the earth surface to the value outside the atmosphere. The weighing coefficient for each band is computed as the ratio of radiation flux at the top of the atmosphere for a particular band to the radiation flux at the top of the atmosphere for all bands.

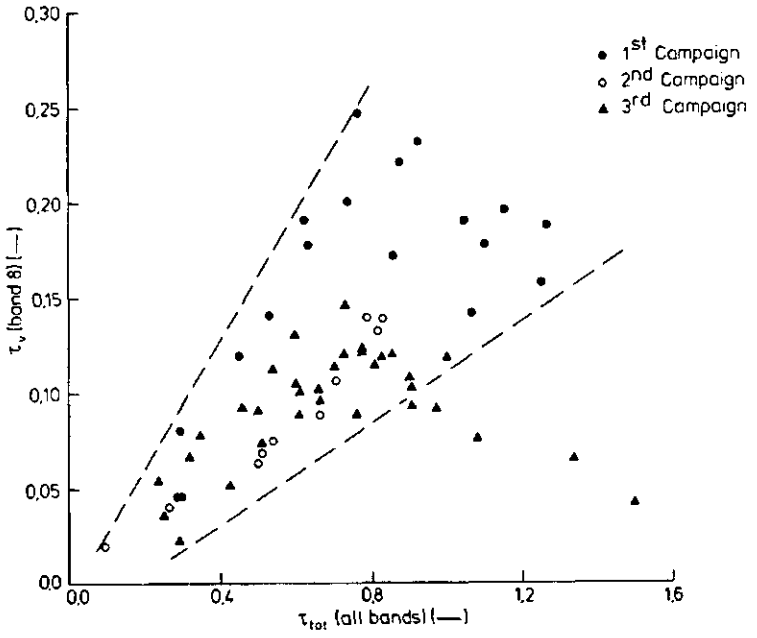

Fig 3.4. Optical depth due to water vapour (band 8), $\tau_{v(band\ 8)}$ versus the total optical depth of all bands, $\tau_{tot(all\ bands)}$; measurements as obtained by means of the rotating band spectroradiometer

As stated we are looking for a relationship between τ_v and τ_{tot}. Since the water vapour band lies in the spectral range of band 8, it is recommended to relate $\tau_{tot(all\ bands)}$ with $\tau_{v(band\ 8)}$ directly. All other bands indicate that τ_v is always lower than 0.008. The result of an attempt to relate the mentioned optical depths from July 1986 through November 1987 is shown in Fig 3.4.

In order to predict $\tau_{v(band\ 8)}$ from $\tau_{tot(all\ bands)}$, the range between τ_v = 0.01-0.10 only appears trustworthy. Hence, with transparent atmospheres the transmittance is governed by the vapour content.

3.4. THE APPLICATION OF REMOTE SENSING DATA TO MAP NET RADIATION

A manner to relate apparent emissivity with atmospherical and meteorological variables, was shown in the preceding sections.

The areal distribution of net radiation can now be predicted. The computation scheme can be briefly summarized as shown in Table 3.7.

It appears that the solar radiation at the bottom of the atmosphere (global radiation) has to be accurately known. The only way to face that difficulty is the use of calibrated pyranometers. Global radiation data have a twofold

Table 3.7. Alternative procedures for the estimation of net radiation

Option	Remote sensing	Meteorological observations	Atmospherical conditions	Apparent emissivity	Day(d) nigth(n)
1a	α_0, T_0	R_{sw}, T_a, RH	-	$\epsilon' = 0.72 + 0.046\sqrt{e_{act}}$	d
1b	T_0	T_a, RH	-	$\epsilon' = 0.61 + 0.068\sqrt{e_{act}}$	n
2a	T_0	T_a	-	$\epsilon' = 0.149.10^4\ T_a^{-1.318}$	n
2b	T0	*	-	$\epsilon' = 0.149.10^4\ T_a^{-1.318}$	n
3a	α_0, T_0	R_{sw}, T_a	$\bar{\tau}_{tot}$	$\epsilon' = 1.08\ \bar{\tau}_{tot}^{0.265}$	d
3b	α_0, T_0	R_{sw},*	$\bar{\tau}_{tot}$	$\epsilon' = 1.08\ \bar{\tau}_{tot}^{0.265}$	d
4a	α_0, T_0	R_{sw}, T_a	$\bar{R}_{swdf}/\bar{R}_{sw}$	$\epsilon' = 0.84 + 0.167\bar{R}_{swdf}/\bar{R}_{sw}$	d
4b	α_0, T_0	R_{sw},*	$\bar{R}_{swdf}/\bar{R}_{sw}$	$\epsilon' = 0.84 + 0.167\bar{R}_{swdf}/\bar{R}_{sw}$	d

*air temperature estimated from surface temperature

application to obtain the net shortwave radiation and the optical depth of the atmosphere. Further, the air temperature can eventually be derived from the surface temperature, because the diurnal variation of the temperature stratification was rather constant during the field campaigns and T_0-T_a was on average 8.7°C at the local satellite overpass time for the fourth field campaign. When thermal infrared images are applied to map net radiation, the difference between at-surface and at-satellite temperature caused by absorption and emission, should be evaluated which at the same time is an excellent chance to asses the apparent emissivity from the atmospheric vapour contribution.

This calculation can be done by means of radiation transfer models (PRICE, 1977).

It is recommended to apply option 1a (Table 3.7) when sufficient meteorological data are available. For the night values of net radiation, alternative 2a is satisfactory. Computations of apparent emissivity can also be done through the optical depth approach (option 3a). Attention has to be given to the different defenitions of the optical depth. A combination of the alternatives will be often possible.

4. SOIL HEAT FLUX

4.1 REVIEW

The soil heat flux represents the soil heat exchange component of the energy budget (see eq. [2.1]). The expression of the vertical conductive heat flow reads:

$$G = - \lambda \frac{\partial T}{\partial z} \qquad [4.1]$$

where: G = soil heat flux ($W.m^{-2}$)
T = soil temperature (K)
z = vertical distance (m)
λ = thermal conductivity ($W.m^{-1}.K^{-1}$)

The soil heat flux is depth dependent because of heat storage, which implies that temperature waves will not penetrate equally along the soil profile; moreover thermal conductivity is varying with soil water content. The soil heat flux at surface level should therefore be related with the soil temperature gradient at a particular depth. In this study, the temperature gradient between surface level and 10 mm depth will be considered.
Profiles of soil temperature depend besides the flux density, on the soil heat capacity C ($J.m^{-3}.K^{-1}$). The latter property describes the change of temperature in reaction to a change in heat storage, which can be formulated in combination with the principle of continuity, saying that the difference in heat flux through an arbitrary layer equals the rate of change in heat storage::

$$C \frac{\partial T}{\partial t} = \frac{\partial}{\partial z}(\lambda \frac{\partial T}{\partial z}) \qquad [4.2]$$

Due to scarcity of information on actual gradients of soil temperature, the surface energy balance applied in evapotranspiration equations is often for practical reasons simplified by excluding the soil heat term. This leads to an overestimation of the latent heat flux, especially when only evaporation from the barren soil has to be assessed. Neglecting of the soil heat flow

in arid regions will create a serious drawback on the estimations of the other terms of the energy balance and requires a careful approach.
A practical solution to account for soil heat flow can be sought in a manner by relating soil heat flux to net radiation by means of simple, empirical relationships e.g. $G_0 = 0.1\ R_n$ (DE BRUIN and HOLTSLAG, 1982). The determination of such functions requires a indepth study as presented in this chapter.

4.2. COMPARISON OF LINEAR RELATIONSHIPS BETWEEN NET RADIATION AND SOIL HEAT FLUX

During fieldwork, in situ measurements of G_0.T_0 and $\partial T_s/\partial z$ were performed at five different locations inside the Qattara depression (Table 4.1). The soil heat flux G_0 was always measured by means of two soil heat flux plates, located at 2 different depths. The observed fluxes were recorded with a 5 minute interval. The plates were installed as shallow as possible, just some millimeters under the surface. The surface temperature (T_0) was measured by means of a thermal infrared radiometer. Soil temperature values along the vertical profile were obtained with a switchable thermistor device and registrated every 60 minutes.
In order to investigate the relevance of the soil heat flux in the radiation budget, values of net radiation were collected simultaneously with the soil heat flux data (Fig. 4.1). The dependence of soil heat flux on net radiation is evaluated by the correlation coefficient as presented in Table 4.2. A discrimination between morning (< 13.30 h) and afternoon values was made to study the warming up and cooling down processes.
If the morning values on 11/6 and the afternoon values on 25/6 are neglected, the overall correlation coefficient becomes r = 0.98 while 44%

Table 4.1. Soil heat flux observations; fieldwork 1988

Date	Location	Soil
10-13/6/88	Bir Qifar-1	Dark brown dry puffy
14-16/6/88	Bir Qifar-2	Dry sandy puffy
17-19/6/88	Bir Qifar-3	Dry puffy with salt traces
20-22/6/88	Bir Qifar-4	Porous clayey puffy
23-25/6/88	Bir Qifar-5	Rough hummocky with polygons

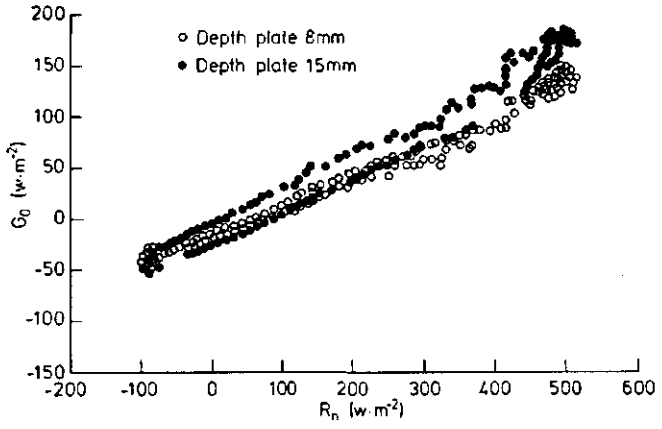

Fig. 4.1. Observed soil heat flux, G_0 against net radiation, R_n: Bir Qifar-3 18 June 1988

Table 4.2. Correlation coefficients between soil heat flux G_0 and net radiation R_n. G_0 was measured by means of two different transducers (Plate 1, 2) at different depths

Day	Site	Morning		Afternoon		Depth (mm)	
		plate 1	plate 2	plate 1	plate 2	plate 1	plate 2
11/6	1	0.596	0.530	0.986	0.978	12	17
12/6	1	0.989	0.993	0.924	0.905	12	17
13/6	1	0.996	0.999	-	-	12	17
14/6	2	0.863	0.935	0.979	0.978	9	13
15/6	2	0.994	0.997	0.991	0.989	9	13
16/6	2	0.984	0.987	-	-	9	13
17/6	3	0.957	0.985	0.979	0.958	8	15
18/6	3	0.997	0.989	0.992	0.996	8	15
19/6	3	0.994	0.990	-	-	8	15
20/6	4	0.948	0.954	0.998	0.987	10	10
21/6	4	0.998	0.997	0.991	0.976	10	10
22/6	4	0.948	0.956	-	-	10	10
23/6	5	0.933	0.964	0.985	0.992	12	10
24/6	5	0.997	0.992	0.991	0.996	12	10
25/6	5	0.994	0.991	0.627	0.619	12	10

of the correlation coefficients were higher than r = 0.99. Hence, it can be concluded that it is possible to establish a relationship between G_0 and R_n. The high correlation was noticed for both soil heat flux plates. The similar morning and afternoon correlation coefficients seem to imply that the phase difference between R_n and G_0 can be neglected. This also states that the selected depths of the soil heat flux plates (8-15 mm) were appropriate to measure G_0 as the soil heat flux at the soil surface. To investigate the role of G_0 against R_n more deeply, a regression analysis has been performed. The determined regression coefficients are listed in Table 4.3.

Table 4.3A. Linear regression coefficients of $G_0 = a + b\ R_n$ ($W.m^{-2}$); plate 1, where G_0 ($W.m^{-2}$) is the soil heat flux and R_n ($W.m^{-2}$) the net radiation

Date	Site	Depth (mm)	Morning		Afternoon		$\bar{G}_0/\bar{R}_n$
			a	b	a	b	
11/6	1	12	-16.2	0.126	-19.2	0.168	0.129
12/6	1	12	-27.6	0.238	- 8.9	0.209	0.189
13/6	1	12	-27.8	0.228	-	-	0.170
14/6	2	9	- 6.3	0.322	- 1.3	0.358	0.347
15/6	2	9	-26.1	0.371	- 1.1	0.301	0.297
16/6	2	9	- 6.4	0.311	-	-	0.303
17/6	3	8	- 0.2	0.261	-44.5	0.334	0.248
18/6	3	8	-13.4	0.297	-15.3	0.272	0.251
19/6	3	8	-10.8	0.312	-	-	0.293
20/6	4	10	-15.4	0.292	-45.6	0.347	0.307
21/6	4	10	-32.4	0.392	-50.3	0.339	0.315
22/6	4	10	-17.5	0.339	-	-	0.277
23/6	5	12	-27.5	0.191	-30.9	0.158	0.130
24/6	5	12	-28.5	0.155	-26.4	0.152	0.104
25/6	5	12	-24.9	0.181	-26.0	0.191	0.138

Table 4.3B. Linear regression coefficients of $G_0 = a + b\ R_n$ ($W.m^{-2}$); plate 2, where G_0 ($W.m^{-2}$) is the soil heat flux and R_n ($W.m^{-2}$) the net radiation

Date	Site	Depth (mm)	Morning		Afternoon		$\bar{G}_0/\bar{R}_n$
			a	b	a	b	
11/6	1	17	-10.1	0.103	-18.4	0.163	0.119
12/6	1	17	-26.3	0.226	- 2.5	0.181	0.178
13/6	1	17	-22.9	0.231	-	-	0.173
14/6	2	17	-27.7	0.373	- 0.6	0.295	0.298
15/6	2	13	-20.3	0.326	+ 0.3	0.245	0.258
16/6	2	13	- 3.9	0.301	-	-	0.298
17/6	3	15	-40.4	0.382	-22.2	0.355	0.297
18/6	3	15	-24.0	0.371	- 9.5	0.363	0.325
19/6	3	15	-19.0	0.336	-	-	0.301
20/6	4	10	+12.4	0.303	-61.0	0.350	0.300
21/6	4	10	-32.0	0.419	-61.7	0.355	0.343
22/6	4	10	-12.3	0.372	-	-	0.324
23/6	5	10	-57.2	0.279	-32.6	0.212	0.166
24/6	5	10	-34.9	0.197	-27.4	0.215	0.162
25/6	5	10	-31.0	0.237	+ 4.9	0.211	0.192

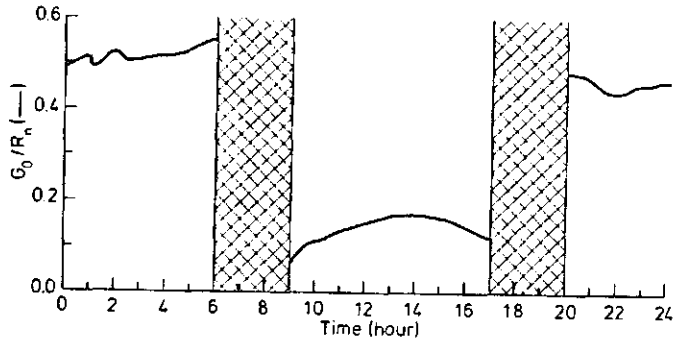

Fig. 4.2. Diurnal variation of G_0/R_n for all sites: Bir Qifar-5 24 June 1988

A statistical t-test is done, to assess whether $a,b_{(morning)}$ are significantly different from $a.b_{(afternoon)}$. Considering 42 degrees of freedom and a probability level of 95%, the a-coefficients appear not to be statistically different (t-value = 0.28). The t-value for the b-coefficients (t-value = 0.42) indicates the same result. The differences between $a.b_{(morning)}$ and $a.b_{(afternoon)}$ are therefore, not significant. To be precise, the next step is to obtain the mean ratio of G_0 to R_n during daytime, because evapotranspiration is often considered on a daily basis. In order to do so, the daily $\overline{G_0}/\overline{R_n}$ ratio has been determined and added to Table 4.3. An example of the diurnal variation of G_0/R_n is illustrated in Fig 4.2. The ratio G_0/R_n varies between 10 and 35% during daytime. Hence, soil heat exchange can be a major component of energy that is absorbed by the surface.

4.3. PHYSICAL ANALYSIS OF THE RELATIONSHIP BETWEEN NET RADIATION AND SOIL HEAT FLUX

4.3.1. General

The thermal conductivity and thermal capacity are linked up in some thermal expressions, such as thermal diffusivity (λ/C), diurnal heat capacity $(\Omega C\lambda)^{0.5}$, thermal admittance $(\Omega C\lambda)^{0.5} \exp i\pi/4$ and thermal inertia $(C\lambda)^{0.5}$. The term Ω accounts for the angular frequency of the temperature wave which equals to 2π/Period (rad.s^{-1}).

The aim of this section is to verify whether the ratio $\overline{G_0}/\overline{R_n}$ is dependent on the soil thermal properties or not. Therefore as a first check, observed values of soil thermal properties are compared with values obtained on

basis of the volumetric contribution of the different soil constituents. The second step is to relate the soil thermal properties with $\overline{G}_0/\overline{R}_n$.

4.3.2. Thermal conductivity

The thermal conductivity (λ) can directly be derived by inversion of eq. [4.1]. The comparison of thermal conductivity values can only be done when they apply to a same soil-depth, e.g. the toplayer between 0 and 10 mm. The average differential of thermal conductivity towards depth as derived from the puffy soils of site 2 and 3 has been applied ($\partial\lambda/\partial z$ = -11.4 $W.m^{-2}.K^{-1}$) in order to obtain values for λ in the 0-10 mm layer of site 1. Table 4.4 gives the results obtained with both plates.
The measured values of λ do not resemble very precisely the expected λ-values (Table 4.5), as calculated by means of the formula proposed by DE

Table 4.4. Values of thermal conductivity observed by means of plate 1 (λ_1) and plate 2 (λ_2). The average thermal conductivity between 0 and 10 mm (λ(10 mm)) is presented

Date	Site	Number of datapoints	Depth 1 (mm)	λ_1 ($W.m^{-1}.K^{-1}$)	Depth 2 (mm)	λ_2 ($W.m^{-1}.K^{-1}$)	(10 mm) ($W.m^{-1}.K^{-1}$)
11/6	1	70	15	0.314	15	0.314	0.371
12/6	1	87	15	0.372	15	0.372	0.429
13/6	1	6	15	0.658	15	0.658	0.715
14/6	2	81	9	0.521	13	0.443	0.502
15/6	2	93	9	0.532	13	0.455	0.513
16/6	2	13	9	0.445	13	0.436	0.444
17/6	3	86	8	0.443	15	0.370	0.422
18/6	3	87	8	0.441	15	0.330	0.410
19/6	3	10	8	0.387	15	0.378	0.384
20/6	4	75	10	0.665	10	0.645	0.655
21/6	4	60	10	0.669	10	0.697	0.683
22/6	4	13	10	0.222	10	0.259	0.241
23/6	5	30	12	1.392	10	1.563	1.563
24/6	5	49	12	0.500	10	0.741	0.741
25/6	5	76	12	0.753	10	0.979	0.979

Table 4.5. Observed and calculated thermal conductivity (λ)

Site	Soil water Content ($cm^3.cm^{-3}$)	Porosity ($cm^3.cm^{-3}$)	Halite content ($cm^3.cm^{-3}$)	Observed λ ($W.m^{-1}.K^{-1}$)	Calculated λ ($W.m^{-1}.K^{-1}$)
1	0.114	0.40	0.10	0.42	0.33
2	0.043	0.45	0.05	0.50	0.41
3	0.040	0.40	0.10	0.41	0.52
4	0.073	0.50	0.15	0.63	0.27
5	0.085	0.30	0.10	0.89	0.58

VRIES (1963). It should be taken into account that De Vries assumed that soil particles do not interact thermally with each other. As a consequence, the weighing coefficients accounting for the shape of each granule and the ratio between the thermal conductivities of each particle are uncertain. Furthermore, experiments indicated that with lower soil water contents, the soil air has to be considered as the surrounding medium, which induces another source of difficulties (FEDDES, 1971, TEN BERGHE, 1986). The determination of λ was based on in situ measurements of soil water content. It appeared that the total porosity has much more influence than the soil salinity on the thermal conductivity. Although methods to estimate λ are useful, indirect measurements (e.g. on the basis of eq. [4.1] look more successful. The measured conductivity of site 5, is significantly higher than the measured conductivity at the other locations.

With regard to the validity of the calculated λ values, it must be emphasized that the measured conductivity has in most cases, except site 3, a higher value than the calculated conductivities. Further, the observed hourly values of λ showed that λ is certainly not constant (Fig. 4.3). Variations and even peaks can be noticed, which can be due to thermal convective flow of soil air; the apparent conductivity (100 %) accounts for both conductive (75 %) and convective (25 %) heat flow, where the velocity of convective soil air displacement (V_{za}) can be described as a supplementary term (Menenti, 1984).

$$\lambda' = \lambda^* + \rho_a C_p |V_{za}| \delta z \qquad [4.3]$$

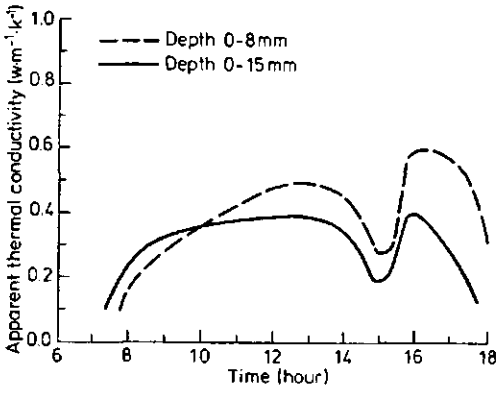

Fig. 4.3. Observed hourly values of apparent thermal conductivity; Bir Qifar-3, 18 June 1988

Thermal convection occurs when the density of moist air at the evaporation front is lower than at the surface. This is very obvious at 16.00 hour, when the soil temperature is maximally. The minimum rate of moist air convection is obtained at 15.00 hour, when the surface temperature is maximally and differences in soil air density due to humidity are compensated by soil temperature.
Hence, values of λ' determined in situ, were somewhat higher than λ^* values computed by de Vries method, and the difference between the λ values can be explained by soil air convection.

4.3.3. Thermal diffusivity

When the surface temperature is written as a sinusoidal function of time (CARSLAW and JAEGER, 1959), which approximation is acceptable in arid regions (Fig. 4.4), a damping depth (d) can be defined, being the depth where the amplitude of temperature is a fraction e^{-1} of the amplitude at the soil surface:

$$A(z) = A(0)\ e^{-z/d} \qquad [4.4]$$

Further, the damping depth (d) can be related to the thermal diffusivity (a) according:

$$d = (2\ a/\Omega)^{0.5} \qquad [4.5]$$

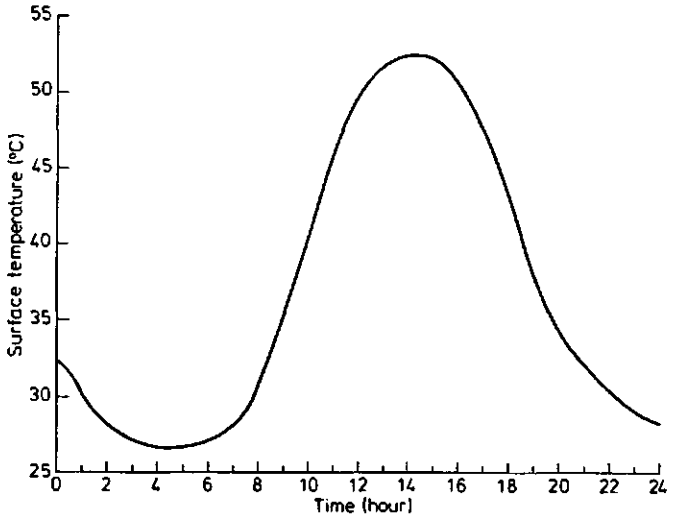

Fig. 4.4. Diurnal variation of surface temperature; Bir Qifar-4 21 June 1988

Table 4.6. Observed depth dependent thermal diffusivity, $a_i(z_i)$

Day	Site	$(m^2.s^{-1}).10^{-6}$				(cm)			
		a1	a2	a3	a4	z1	z2	z3	z4
10/6	1	0.009	0.076	0.138	0.209	0.9	4.0	6.4	12.6
11/6	1	0.016	0.138	0.211	0.256	0.9	4.0	6.4	12.6
12/6	1	0.020	-	0.134	0.208	1.5	4.0	6.4	12.6
14/6	2	0.050	0.108	0.148	0.362	2.0	3.0	4.0	9.0
15/6	2	0.064	0.125	0.157	0.376	2.0	3.0	4.0	9.0
17/6	3	0.153	0.667	0.408	0.880	2.5	5.0	7.6	10.5
18/6	3	0.109	0.282	0.338	0.600	2.5	5.5	7.6	10.5
20/6	4	0.137	0.573	0.329	0.268	1.0	3.0	5.0	30.0
21/6	4	0.266	0.396	0.312	0.208	1.0	3.0	5.0	30.0
23/6	5	0.383	0.412	0.818	1.070	2.0	4.3	8.0	12.0
24/6	5	0.188	0.316	0.612	0.852	2.0	4.3	8.0	12.0

Combination of eq. [4.4] and eq. [4.5] yields:

$$a = \frac{\Omega}{2} z^2/(\ln A(0) - \ln A(z))^2 \qquad [4.6]$$

Advantage of this approach is that only soil temperature measurements at two depths are required to estimate the soil thermal properties. Results of this method are presented in Table 4.6.
The concept of damping depth can only be applied to homogeneous soil profiles. The data in Table 4.6 for one location indicate that thermal diffusivity varies with depth; low values near the surface and higher values deeper along the profile. It is known that thermal diffusivity changes with soil water content, since both λ' and C depend on soil water content. Hence, the damping depth may not be considered as a constant.

4.3.4. Thermal admittance

Remote sensing investigations on the energy balance at the earth surface require a clear relationship between the soil heat flux and surface temperature. MENENTI (1984) proposed to this purpose the concept of thermal admittance (Y_0) at the surface of a not homogeneous soil:

$$Y_0 = G_0(t)/T_0(t) \qquad [4.7]$$

with

$$Y_0 = (C\lambda'\Omega)^{0.5} \exp i\pi/4 \qquad [4.8]$$

Table 4.7. Values of thermal admittance observed by two transducers at different depths ($Y_{0.1}$ and $Y_{0.2}$) and transfered to the layer between 0 and 10 mm ($Y_{0.10\ mm}$)

Day	Site	$Y_{0.1}$ ($W.m^{-2}.K^{-1}$)	$Y_{0.2}$ ($W.m^{-2}.K^{-1}$)	$Y_{0.10\ mm}$ ($W.m^{-2}.K^{-1}$)	z_1 (mm)	z_2 (mm)
11/6	1	8.34	8.34	9.20	15	15
12/6	1	6.53	6.53	7.39	15	15
14/6	2	6.63	5.53	6.31	9	13
15/6	2	6.29	5.63	6.13	9	13
17/6	3	7.89	6.83	7.59	8	15
18/6	3	6.85	5.52	6.49	8	15
20/6	4	7.48	7.73	7.61	10	10
21/6	4	10.90	11.77	11.34	10	10
23/6	5	6.80	8.54	8.54	12	10
24/6	5	4.64	6.08	6.08	12	10

The modulus of the thermal admittance $(C\lambda'\Omega)^{0.5}$ may then be obtained with the daily amplitude of the surface temperature and flux:

$$(C\lambda'\Omega)^{0.5} = A(G_0)/A(T_0) \qquad [4.9]$$

This has been done with our measurements of surface temperature and soil heat flux. Because of the shallow depth of the plates, the profile can be considered as being homogeneous. Due to the unequal depths of the plates, different values of the thermal admittance were determined. As stated before, G_0 was valid for the 0-10 mm layer, so that Y_0 values have to be transferred to this reference depth. The transformation for site 1 has been done by applying $\partial Y_0/\partial z = -171\ W.m^{-1}.K^{-1}$.

4.3.5. Soil heat capacity

The soil heat capacity (C) can be assessed by means of the thermal diffusivity or the thermal admittance, when the thermal conductivity is known. Let us assume that the apparent conductivities of Paragraph 4.2.2 are right, then C-values can be derived from respectively a-values and Y_0-values and compared with theoretical values calculated by means of the following formula:

$$C = (x_{Sio2}\ 2.01 + x_{Na}\ 0.90 + x_w\ 4.40).10^6 \qquad [4.10]$$

where x_{Sio2} (-) = volumetric fraction of quartz
x_{Na} (-) = volumetric fraction of halite
x_w (-) = volumetric fraction of water

The volumetric heat capacities ($J.m^{-3}.K^{-1}$) of soil constituents are 2.01, 0.90 and 4.40 respectively. The volumetric fractions of constituents in eq. [4.10] are equal to the values applied for the determination of the thermal conductivity (see Table 4.5). The results obtained by means of by the thermal admittance method indicate a better correspondence with the C-values calculated by means of eq. 4.12 than results obtained by means of the damping depth method. However, if the diffusivity values of deeper layers only are applied (see Table 4.9), the resulting soil heat capacities fit better with C-values calculated by means of eq. [4.10]

Hence, the thermal admittance approach appears useful to obtain the soil thermal properties when the surface temperature and soil heat flux are known. If only observations of soil temperature are available, the soil thermal properties can be derived on the basis of observed thermal diffusivity.

Reference values of a can be obtained by dividing λ'-values in Table 4.4 by the corresponding C-values, as calculated by means of eq. [4.10].

The method of the thermal diffusivity to obtain C appears only suitable if the temperature is measured at sub-surface level i.e. between 3 and 12 cm depth. So, soil temperature recordings at say 65% of the damping depth

Table 4.8. Soil heat capacity, C in playa areas: site 1-5 July 1988, calculated according the thermal admittance concept, $C(Y_0)$, the damping depth concept, C(a) and eq. [10], C(eq. [10])

Day	Site	Depth (mm)	λ' ($W.m^{-1}.K^{-1}$)	($J.m^{-3}.K^{-1}$).10^6		
				$C(Y_0)$	C(a)	C(eq.10)
11/6	1	0-15	0.314	3.05	2.03	1.60
12/6	1	0-15	0.372	1.58	3.07	1.60
14/6	2	0- 9	0.521	1.16	3.12	1.24
14/6	2	0-13	0.443	0.89	2.65	1.24
15/6	2	0- 9	0.532	1.02	2.94	1.24
15/6	2	0-13	0.455	0.96	2.51	1.24
17/6	3	0- 8	0.443	1.93	0.84	1.27
17/6	3	0-15	0.370	1.73	0.70	1.27
18/6	3	0- 8	0.441	1.46	1.33	1.27
18/6	3	0-15	0.330	1.27	0.99	1.27
20/6	4	0-10	0.665	1.16	2.03	1.16
20/6	4	0-10	0.645	1.27	1.97	1.16
21/6	4	0-10	0.669	2.44	2.27	1.16
21/6	4	0-10	0.697	2.73	2.36	1.16
23/6	5	0-12	1.392	0.46	2.07	1.67
23/6	5	0-10	1.563	0.65	2.33	1.67
24/6	5	0-12	0.500	0.59	1.02	1.67
24/6	5	0-10	0.741	0.69	1.51	1.67

Table 4.9. Corrected thermal diffusivity a apparent thermal conductivity λ', thermal capacity C(a) obtained from $C = \lambda'/a$, thermal capacity C (eq. 10) calculated by means of eq. [10] and thermal diffusivity d

Date	Site	Depth (z) (cm)	a 10^{-6} ($m^2.s^{-1}$)	λ' ($W.m^{-1}.K^{-1}$)	($J.m^{-3}.K^{-1}$)		d (cm)	z/d (-)
					C(a)	C(eq. 10)		
11/6	1	6.4	0.211	0.314	1.49	1.60	7.6	1.19
12/6	1	12.6	0.208	0.372	1.79	1.60	7.6	0.60
14/6	2	9.0	0.362	0.521	1.44	1.24	10.0	0.90
14/6	2	9.0	0.362	0.443	1.22	1.24	10.0	0.90
15/6	2	9.0	0.376	0.532	1.41	1.24	10.2	0.88
15/6	2	9.0	0.376	0.455	1.21	1.24	10.2	0.88
17/6	3	7.6	0.408	0.443	1.09	1.27	11.6	0.72
17/6	3	7.6	0.408	0.370	0.91	1.27	11.6	0.72
18/6	3	7.6	0.282	0.441	1.56	1.27	8.8	0.86
18/6	3	7.6	0.282	0.330	1.17	1.27	8.8	0.86
20/6	4	3.0	0.573	0.665	1.16	1.16	12.2	0.25
20/6	4	3.0	0.573	0.645	1.20	1.16	12.2	0.25
21/6	4	3.0	0.396	0.669	1.69	1.16	10.4	0.29
21/6	4	3.0	0.396	0.697	1.76	1.16	10.4	0.29
23/6	5	12.0	1.070	1.563	1.46	1.67	17.2	0.70
23/6	5	8.0	0.818	1.392	1.70	1.67	15.0	0.53
24/6	5	4.3	0.316	0.741	1.40	1.67	9.3	0.46
24/6	5	4.3	0.316	0.500	1.58	1.67	9.3	0.46

Table 4.10. Observed thermal diffusivity a and damping depth d

Day	Location	soil	a ($m^2.s^{-1}$).10^{-6}	d (cm)
26/2/87	Bir Tarfawi	Bare coarse sand	0.55	12.3
9/3/87	Siwa oasis East	Dark brown hummocky	0.45	11.1
9/3/87	Siwa oasis East	White puffy	0.20	7.3
9/3/87	Siwa oasis East	Grey brown puffy	0.71	14.0
11/3/87	Siwa oasis West	Hummocky-1	0.24	8.1
11/3/87	Siwa oasis West	Hummocky-2	0.20	7.4
12/3/87	Siwa oasis West	Hummocky-1	0.30	9.0
12/3/87	Siwa oasis West	Hummocky-2	0.27	8.6
14/3/87	Siwa oasis East	Hummocky	0.83	15.1
15/3/87	Siwa oasis East	Hummocky	0.97	16.3
4/11/87	Qara oasis	Hummocky	1.09	17.3
8/11/87	Qattara	Brown puffy	0.38	10.1
11/11/87	Qaneitra	Grey brown puffy	0.19	7.1
12/11/87	Qaneitra	Grey brown puffy	0.24	7.9

(z/d) is a rule of thumb to get proper values of the thermal diffusivity. The effect of the high frequency thermal variability in the heterogeneous toplayer is then eliminated. This is essentially true for small damping depths. The a-values (at a depth 65% of d) obtained with field measurements, given in Table 4.10 provide an impression of the variability of thermal properties in playas

4.3.6. Discussion

A large thermal conductivity and a large temperature gradient cause deeper penetration of heat into the soil. If the heat capacity increases with depth, the temperature amplitude will decrease rapidly at deeper depths and a driving thermal gradient will remain. Thus a large value of the product of conductivity and capacity enables a relatively large soil heat flow, while a large diffusivity, with consequently a low heat capacity, gives rapid changes of soil temperature only. Table 4.11 illustrates the relationship between the ratio $\bar{G}_0/\bar{R}_n$ and soil thermal properties. If G_0 is considered as the surplus of the energy budget at the earth surface, with a restricted sensible (and latent) heat flux, $\bar{G}_0/\bar{R}_n$ increases with net radiation. Another possibility is that soil heat flow is limited by the molecular conduction and convection so that $\bar{G}_0/\bar{R}_n$ decreases with increasing net radiation. Net radiation is mainly governed by the net

Table 4.11. Observed relationship between soil heat and net radiation flux $\bar{G}_0/\bar{R}_n$ versus the soil thermal properties like thermal admittance Y_0 and thermal diffusivity a. Also the normalized surface reflectance α''_0 is presented

Source:		Table 4.3	Table 4.7	Table 4.9	-
Date	Site	$\bar{G}_0/\bar{R}_n$ (0-10 mm) (-)	Y_0 (0-10 mm) ($W.m^{-2}.K^{-1}$)	a (3-12 cm) ($m^2.s^{-1}$).10^{-6}	α''_0 (-) (-)
11-6	1	0.133	9.20	0.211	0.185
12-6	1	0.193	7.39	0.208	0.195
14-6	2	0.335	6.31	0.362	0.300
15-6	2	0.287	6.13	0.376	0.289
17-6	3	0.262	7.59	0.408	0.191
18-6	3	0.272	6.47	0.282	0.184
20-6	4	0.304	7.61	0.573	0.179
21-6	4	0.329	11.34	0.396	0.178
23-6	5	0.166	8.54	0.944	0.156
24-6	5	0.162	6.08	0.316	0.155

shortwave radiation, i.e. global incoming radiation minus reflected radiation. The effect of surface reflectance on net radiation and soil heat flux has therefore to be considered: with increasing reflectance, net radiation will decrease, so that $\overline{G}_0/\overline{R}_n$ increase at constant G_0. In this respect it may be interesting to relate G_0 either R_n, surface reflectance (α_0) or with bulk soil thermal properties (λ', C). Surface reflectance shows, however, a diurnal variation.

Observed values, α_o, at any time or under any atmospheric conditions have to be normalized by defining a reference sun zenith angle and reference atmospheric conditions (BASTIAANSSEN, 1988).

The normalized surface reflectance applies to a sun zenith angle of 0°, absence of dew and an optical depth of Earth's atmosphere $\tau_{tot} = 0.6$.

The data points in Figure 4.5 indicate a clear correlation between $\overline{G}_0/\overline{R}_n$ and thermal diffusivity. No correlation was observed between $\overline{G}_0/\overline{R}_n$ and thermal admittance. In principle, there should be a relationship between $\overline{G}_0/\overline{R}_n$, surface reflectance α''_o and thermal diffusivity a. At constant G_0, R_n decreases with increasing α''_o, so $\overline{G}_0/\overline{R}_n$ will increase. Data points having $\alpha''_0 = 0.300$, 0.289 and 0.190 support this concept, while others do not. However, when using mean values for one soil type, the role of surface reflectance is evident (Table 4.12).

Hence, the effect of surface reflectance is superimposed on the effect of a on $\overline{G}_0/\overline{R}_n$ (Figure 4.6). To establish a formula to describe the relationship between G_0, R_n, a and α_o'', a mathematical expresion based on Table 4.11 has

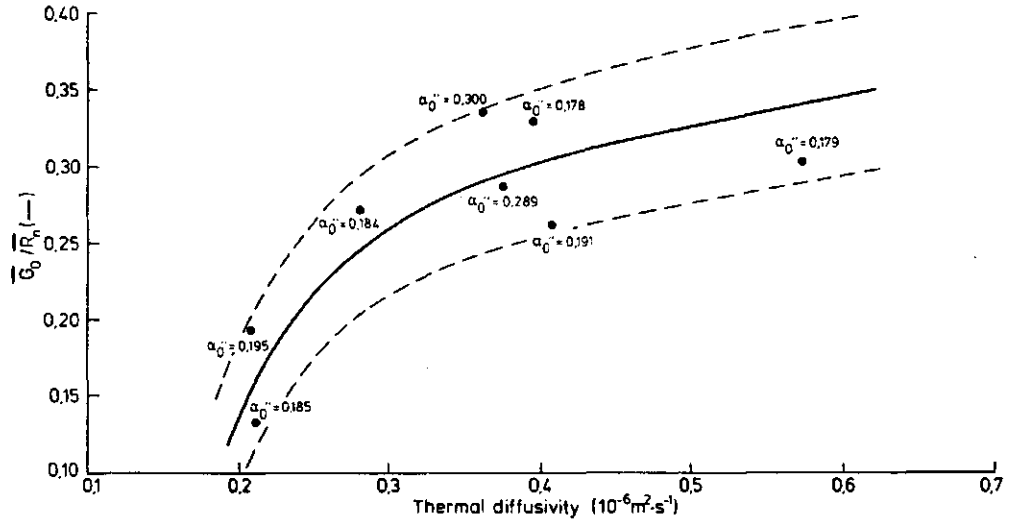

Fig. 4.5. Ratio $\overline{G}_0/\overline{R}_n$ versus thermal diffusivity, a 8 mean daily values for 4 different soil types; for each data point, the normalized surface reflectance, α_o'' is indicated

Table 4.12. Observed playa heat properties, λ', C together with calculated soil heat expressions: thermal diffusivity, a and thermal admittance, γ_0

Site	Soil	α'_0 (-)	λ' (W m^{-1} K^{-1})	C (J m^{-3} K^{-1}) 10^6	a (m^2 s^{-1}) 10^{-6}	γ_0 (W m^{-2} K^{-1})
1	Dark brown dry puffy	0.190	0.415	1.61	0.258	6.97
2	Dry sandy puffy	0.295	0.503	1.19	0.423	6.60
3	Dry sandy puffy with salt crusts	0.189	0.414	1.35	0.307	6.38
4	Porous clayey puffy	0.179	0.630	1.80	0.350	8.29
5	Rough hummocky with polygons	0.186	0.886	1.65	0.537	10.29

to be designed. The relationship between G_0/R_n, thermal diffusivity (a) and normalized reflectance (α''_0) can be described by means of a non-rectangular hyperbola:

$$\bar{G}_0/\bar{R}_n = (0.84\ \alpha''_0 - 0.35).(p - \sqrt{p^2 - 4pp}) \qquad [4.11]$$

with

$$p = 0.993.a - 0.185$$
$$pp = 0.179.a^2 - 0.14.a$$

It is usefull to assess the sensitivity of the ratio $\bar{G}_0/\bar{R}_n$ as calculated by means of eq. [4.11] to surface reflectance α''_0, thermal diffusivity a, and thermal admittance Y_0. Therefore the normalized surface reflectance between $\alpha_0'' = 0.15$ and $\alpha_0'' = 0.35$ as depicted in Fig. 4.6 is considered.

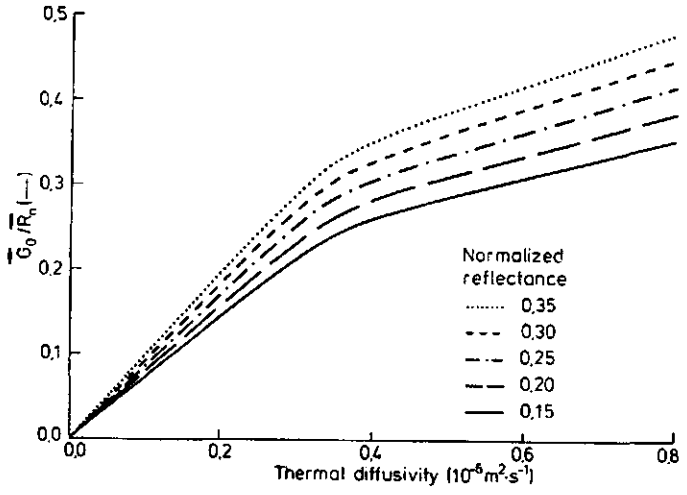

Fig. 4.6. Ratio $\bar{G}_0/\bar{R}_n$ versus thermal diffusivity, a modified by the normalized surface reflectance, α_0''

Table 4.13. Relative variations between cases of $\bar{G}_0/\bar{R}_n$ due to variations in normalized surface reflectance α''_0, thermal diffusivity a, and thermal admittance Y_0

Input				Output			
Site	α''_0 (-)	a $(m^2.s^{-1})10^{-6}$	Y_0 $(W.m^{-2}.K^{-1})$	$\bar{G}_0/\bar{R}_n$ (-)	$\frac{\delta(\bar{G}_0/\bar{R}_n)}{\delta\alpha''_0}$	$\frac{\delta(\bar{G}_0/\bar{R}_n)}{\delta a}$	$\frac{\delta(\bar{G}_0/\bar{R}_n)}{\delta Y_0}$
1	0.15	0.258	6.97	0.184	-	-	-
1	0.35	0.258	6.97	0.249	0.33	-	-
2	0.15	0.423	6.60	0.267	-	0.50	-0.22
2	0.35	0.423	6.60	0.361	0.47	-	-
3	0.15	0.307	6.38	0.217	-	0.43	+0.23
3	0.35	0.307	6.38	0.294	0.39	-	-
4	0.15	0.420	8.29	0.266	-	0.43	+0.03
4	0.35	0.420	8.29	0.360	0.47	-	-
5	0.15	0.537	10.29	0.294	-	0.24	+0.01
5	0.35	0.537	10.29	0.398	0.52	-	-

From the previous table it is clear that the sensitivity of $\bar{G}_0/\bar{R}_n$ to Y_0 is large; a minor change of $\bar{G}_0/\bar{R}_n$ results in a mojor change of Y_0. Vice versa, variations of $\bar{G}_0/\bar{R}_n$ are small in comparison with variations of Y_0. Since the sensitivity of $\bar{G}_0/\bar{R}_n$ to α''_0 and a are higer than to Y_0, the accuracy of the determination of a and α''_0 are quit important. The relative variations of $\bar{G}_0/\bar{R}_n$ due to variations in α''_0 and a differ in general not much. Hence, the effect of surface reflectance on $\bar{G}_0/\bar{R}_n$ can be important as the influence of a on $\bar{G}_0/\bar{R}_n$.

5. LATENT HEAT FLUX

Table 5.1 and 5.2 give a rather accurate estimation of the actual evaporation as measured at the spots in the Qattara depression. As regards the quantitative interpretation, it can be concluded that the order of magnitude of evaporation in playas is much higher (average 0.96 mm.d^{-1}) than the evaporation values given in literature (e.g. JOINT VENTURE QATTARA, 1979). Daily LE-values are calculated according the two procedures mentioned (eq. [2.5] and eq. [2.8]). It may be remarked that if the evaporation front (Z_e) is somewhat deeper, the role of heat storage (W_e) will be more relevant. A simplified estimation of the heat storage can be obtained by the application of next equation:

$$W_e = G_0(1 - e^{-Z_e/d}) \qquad [5.1]$$

The d-values applied are taken from Tables 4.9 and 4.10. The depth of the evaporation front was taken from Figure 5.1, were the relationship between the depth of the groundwater table and the simulated depth of the evaporation front by means of the EVADES model (BASTIAANSSEN, KABAT and MENENTI, 1988) for a medium textured sandy soil is depicted. The soil heat flux leaving the evaporation front (G_e) is monotonicaly estimated as being 15 percent of the soil heat flux leaving the surface (G_0).

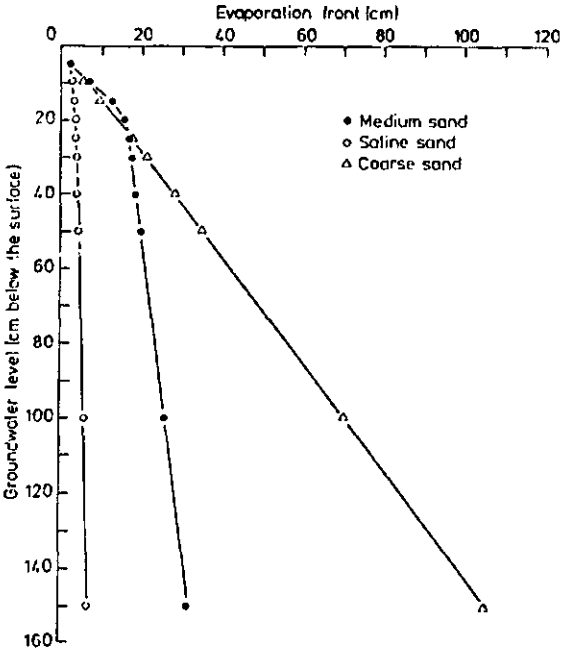

Fig. 5.1. Simulated relationship between groundwater level and depth of the evaporation front by means of the EVADES model for 3 different soil types

Table 5.1. Measured latent heat flux LE; evaporation from the surface without heat storage between the surface and the evaporation front

Date	Site	Water table (cm)	(cal.cm^{-2})		Mean daily evaporation	
			$LE_{(evap.)}$	$LE_{(cond.)}$	(W.m^{-2})	(mm.d^{-1})
15/ 3/87	Siwa oasis	25	118.8	- 3.8	56.0	2.00
16/ 3/87	Siwa oasis	25	126.4	- 3.9	59.5	2.13
5/11/87	Qara oasis	68	139.0	-21.9	56.9	2.03
8/11/87	Qattara	61	103.9	-43.0	29.6	1.06
12/11/87	Siwa oasis	55	61.3	-28.5	15.9	0.57
11/ 6/88	Bir Qifar-1	20	109.5	-27.5	39.8	1.42
12/ 6/88	Bir Qifar-1	20	105.9	-46.3	28.9	1.03
14/ 6/88	Bir Qifar-2	59	116.2	-60.9	26.9	0.96
15/ 6/88	Bir Qifar-2	59	112.4	-62.5	24.3	0.87
17/ 6/88	Bir Qifar-3	43	121.3	-37.5	40.7	1.46
18/ 6/88	Bir Qifar-3	43	123.8	-31.3	45.1	1.61
20/ 6/88	Bir Qifar-4	44	53.7	-27.1	12.9	0.46
21/ 6/88	Bir Qifar-4	44	62.3	-15.9	22.5	0.81
23/ 6/88	Bir Qifar-5	25	74.5	-41.0	16.3	0.58
24/ 6/88	Bir Qifar-5	25	75.8	-44.6	15.2	0.54

Table 5.2. Measured latent heat flux LE; evaporation inside the soil with heat storage between the surface and the evaporation front

Date	Site	Water table (cm)	(cal.cm^{-2})		Mean daily evaporation	
			$LE_{(evap.)}$	$LE_{(cond.)}$	(W.m^{-2})	(mm.d^{-1})
15/ 3/87	Siwa oasis	25	112.3	- 6.4	51.5	1.84
16/ 3/87	Siwa oasis	25	136.9	- 3.8	64.7	2.30
5/11/87	Qara oasis	68	119.7	-35.8	40.8	1.45
8/11/87	Qattara	61	103.9	-43.0	29.6	1.06
12/11/87	Siwa oasis	55	62.7	-22.0	19.7	0.71
11/ 6/88	Bir Qifar-1	20	113.1	-53.7	28.9	1.03
12/ 6/88	Bir Qifar-1	20	115.8	-63.9	25.2	0.90
14/ 6/88	Bir Qifar-2	59	116.2	-60.9	26.9	0.96
15/ 6/88	Bir Qifar-2	59	112.4	-62.5	24.3	0.87
17/ 6/88	Bir Qifar-3	43	146.9	-57.3	43.6	1.56
18/ 6/88	Bir Qifar-3	43	153.5	-53.7	48.5	1.73
20/ 6/88	Bir Qifar-4	44	56.7	-24.8	15.5	0.55
21/ 6/88	Bir Qifar-4	44	61.8	-16.5	22.0	0.79
23/ 6/88	Bir Qifar-5	25	76.0	-46.7	14.3	0.51
24/ 6/88	Bir Qifar-5	25	76.9	-49.3	13.4	0.48

It follows that LE evaluated with the potential and actual evaporation concept differ not much. The experimental differences are inherent with the ratio Z_e/d. When the amount of heat storage in the toplayer is low, i.e. very shallow groundwater, the evaporation determined according eq. [2.8] will be higher than computed according eq. [2.5] (Bir Qifar-1, Bir Qifar-5 and Siwa oasis). When the energy required for heat storage is relatively high, the outcome of eq. [2.8] is not precisely predictable, but the results are close to evaporation values obtained by eq. [2.5].
Furthermore, analyses showed that deposition of dew is an obvious process because an average of 37% of the daily latent heat energy is required for evaporation of dew. This indicates the presence of a daily cyclus of deposition and succesive evaporation of dew. The effect of this deposition-evaporation cyclus was also noticed from measurements of the surface reflectance, where the surface reflectance is much lower in the morning. The latter fact was confirmed by soil moisture analyses. This interactive cyclus between soil and atmosphere has no relation with the evaporation of groundwater.

6. NEW EMPIRICAL ASPECTS OF THE BOWEN-RATIO SURFACE ENERGY BALANCE METHOD

A new method to obtain the soil heat flux from the net radiation, based on field measurements, is outlined in Chapter 4. Thus, instead of considering the soil heat flux as a separate term in the energy balance equation, the soil heat flux can be substituted by the proposed expression of net radiation, thermal diffusivity and surface reflectance (eq. [4.13]). This allows to simplify the Bowen-ratio energy balance method equation. The contribution of the latent heat flux has to be calculated on two different ways which depends on the location of the evaporation front. When the evaporation front is located at surface level, the Bowen-ratio energy balance method (eq. [2.5]) can be simplified according:

$$LE = - \frac{(1-A)\ R_n}{1 + \beta} \qquad [6.1]$$

where

$$A = \overline{G}_0 / \overline{R}_n \qquad [6.2]$$

In cases where the evaporation front is inside the soil (playa), the Bowen-ratio concept is not necessarily required since the latent heat flux is a share of the soil heat flux at the surface (eq. [2.6]). This can be expressed without the Bowen-ratio term. Fluxes towards the evaporation front are counted positive:

$$LE = AR_n - G_e - W_e \qquad [6.3]$$

It is possible to obtain an image of G_0 by means of the procedure to map R_n by remote sensing techniques as outlined in Chapter 3 and the application of eq. [4.13].
Further, when the depth of the evaporation front is known, LE can be assessed from AR_n, G_e and W_e (eq. [6.3]).

7. CONCLUSIONS

- When water evaporates inside the soil, the Bowen-ratio energy balance equation has to be modified with a term for soil heat storage and soil heat flux leaving the evaporation front.
- The Brunt-type formula with new day and nighttime coefficients (eq. [3.5]) is the best alternative to estimate the apparent emissivity.
- With transparent atmospheres, the total optical depth is mainly governed by the purely vapour related optical depth.
- Global radiation has always to be accurately known in order to map net radiation from remote observations of surface reflectance and surface temperature. Ground measurements of air temperature and relative humidity increase the reliability of the results (Brunt-type equation) but are not mandatory to apply the estimation procedure of net radiation.
- The combination of R_{swdf}/R_{sw} and n/N is strongly correlated with dust concentration, rather than with the amount of water vapour.
- The contribution of absorption and re-emittance of thermal infrared radiation can be assessed from the total optical depth by means of the apparent emissivity.
- Observations of soil heat flux against net radiation showed a good correlation ($r = 0.98$).
- In arid regions, soil heat flux can be as large as 10 to 35 % of net radiation.
- The total soil porosity appears to be a crucial parameter in the calculation of the soil thermal properties on the basis of volumetric fractions of soil constituents.
- The soil heat flux is the sum of conduction (75%) and convection (25%).
- Thermal admittance appears useful to derive soil heat properties.
- The damping depth is not constant in the top soil layer (0-30 cm).
- To obtain reliable estimations of the damping depth soil temperature should be measured at depths deeper than 5 cm.
- The estimation of soil heat flux based on the thermal admittance is feasible because a minor change in admittance gives a large difference in soil heat flux with a same soil temperature amplitude.

- Thermal diffusivity in combination with the surface reflectance can be applied to estimate the soil heat flux density directly from net radiation (eq. [4.11]). When the evaporation front is inside the barren soil, the latent heat energy can then be easily estimated from the soil heat flux (eq. [6.3]).
- The daily dew depostion-evaporation cycle takes an important (37%) share of the mean daily latent heat flux.
- Especially with very shallow groundwater, the evaporation determined according to the modified Bowen-ratio approach is slightly larger than the evaporation computed with the classical Bowen-ratio method.
- The mean rate of actual evaporation in playas with a shallow water table (less than 70 cm) is approximately 1 $mm.d^{-1}$.

8. SUMMARY

The areal distribution of evaporation in deserts can be assessed when a relationship between satellite and ground based data is established The actual rate of evaporation can be determined by means of the Bowen-ratio energy balance method. The application of the Bowen-ratio method in arid regions is somewhat questionable, since water will not evaporate from the surface. To face that problem, a modified version of the Bowen-ratio energy balance method is presented. The final results proved that the difference between the alternative procedures in general is not meaningful, but in specific cases can be significantly different (with very shallow groundwater, i.e. less than 30 cm). With the data collected, it was possible to establish new empirical coefficients of known formulae to calculate the apparent emissivity of the atmosphere.
Furthermore, the ratio of soil heat flux and net radiation appeared to be predictable from soil thermal diffusivity and surface reflectance. When the evaporation takes place inside the soil the latent heat flux can be indirectly estimated from the soil heat flux.
Analyses of a number of atmospherical and soil thermal properties were carried out, so that more physical properties of playas are quantitatively known.

Acknowledgements

I am pleased to acknowledge dr. Massimo Menenti for his scientific support and valuable comments on the manuscript of this report.

REFERENCES

BASTIAANSSEN, W.G.M., 1988. Diurnal variation of bare soil reflectance. Note 1854, Institute for Land and Water Management Research (ICW), Wageningen, p. 29.

BASTIAANSSEN, W.G.M., P. KABAT and M. MENENTI, 1988. A new simulation model of bare soil evaporation in arid regions (EVADES). Note 1938, Institute for Land and Water Management Research (ICW), Wageningen. p. 48 (in press).

BERGHE, H.F.M. TEN, 1986. Heat and water transfer at the bare soil surface, Agricultural University, Wageningen, p. 214.

BRUIN, H.A.R., DE, 1982. The energy balance of the earth's surface: a practical approach. W.R. 82-1, Royal Netherlands Meteorological Institute (KNMI), De Bilt, p. 164.

BRUTSAERT, W., 1975. On a derivable formula for longwave radiation from clear skies. Water Resources Research, vol. 2, no. 5. New York, p. 742-744.

CARSLAW, H.S. and J.C. Jaeger, 1959. Conduction of heat in solids. Clarendon Press, Oxford. p. 510.

DOORENBOS and PRUITT, 1977. Crop water requirements, Fao irrigation and drainage paper no. 24, Rome, p. 144 .

FEDDES, R.A., 1971. Water heat and crop growth. Agricultural University, Wageningen. p. 184.

JACKSON, R.D., 1985. Estimating areal evapotranspiration by combining remote and ground-based data. Remote sensing applications for consumptive use. American Water Resources Association, Phoenix, p. 13-23.

JOINT VENTURE QATTARA, 1979. Study Qattara Depression, Vol. 3. Topograhpy, Regional Geology and Hydrogeology. Lahmeyer International.

MENENTI, M., 1984. Physical aspects and determination of evaporation in desert applying remote sensing techniques, Report 10 (special issue), Institute for Land and Water Management Research (ICW), Wageningen. p. 202.

MENENTI, M., 1984. The areal pattern of latent and sensible heat fluxes: the combination of soil physical and remotely sensed data. Integrated Approaches in Remote Sensing, Guildford (ESA SP-214), p. 89-96.